

Heterogeneous & Homogeneous & Bio- & Nano-

# CHEM **CAT** CHEM

---

## CATALYSIS

### Accepted Article

**Title:** Hydroconversion of 5-hydroxymethylfurfural to 2,5-dimethylfuran and 2,5-dihydroxymethyltetrahydrofuran over non-promoted Ni/SBA-15

**Authors:** Shuo Chen, Carmen Ciotonea, Karine Vigier, François Jérôme, Robert Wojcieszak, Franck Dumeignil, Eric Marceau, and Sébastien Royer

This manuscript has been accepted after peer review and appears as an Accepted Article online prior to editing, proofing, and formal publication of the final Version of Record (VoR). This work is currently citable by using the Digital Object Identifier (DOI) given below. The VoR will be published online in Early View as soon as possible and may be different to this Accepted Article as a result of editing. Readers should obtain the VoR from the journal website shown below when it is published to ensure accuracy of information. The authors are responsible for the content of this Accepted Article.

**To be cited as:** *ChemCatChem* 10.1002/cctc.201902028

**Link to VoR:** <http://dx.doi.org/10.1002/cctc.201902028>

# Hydroconversion of 5-hydroxymethylfurfural to 2,5-dimethylfuran and 2,5-dihydroxymethyltetrahydrofuran over non-promoted Ni/SBA-15

Shuo Chen,<sup>[a]</sup> Carmen Ciotonea,<sup>[a]</sup> Karine De Oliveira Vigier,<sup>[b]</sup> François Jérôme,<sup>[b]</sup> Robert Wojcieszak,<sup>[a]</sup> Franck Dumeignil,<sup>[a]</sup> Eric Marceau,<sup>\*,[a]</sup> Sebastien Royer<sup>\*,[a]</sup>

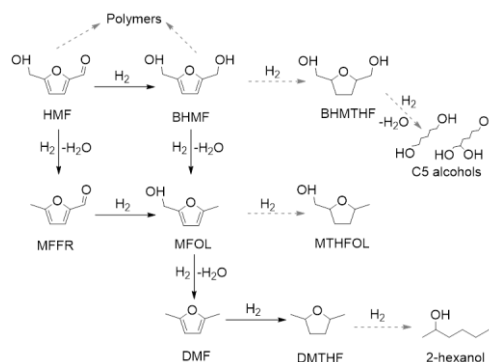
**Abstract:** The selective hydroconversion of 5-hydroxymethylfurfural (HMF) to biofuels is currently highly sought-for. While the literature has demonstrated that this reaction is possible on promoted Ni catalysts, we show here that a monometallic, non-promoted Ni/SBA-15 catalyst, prepared by incipient wetness impregnation, can convert HMF to 2,5-dimethylfuran (DMF) and to 2,5-dimethyltetrahydrofuran (DMTHF) at 180 °C, in a consecutive way. Through a control over reaction time, high yields to DMF (71%, at conversion of 93%) or DMTHF (97%, at conversion of 100%) can be achieved. Kinetic modelling suggests a preferential route to DMF via 5-methylfurfural (MFFR) as intermediate, though the route via 2,5-bis(hydroxymethyl)furan (BHMF) is also present. The favoured route in the experimental conditions involves the hydrogenolysis of the hydroxyl group of HMF as first step, followed by the hydrogenation of the aldehyde function, to methylfurfuryl alcohol (MFOL). It is suggested a higher reaction rate of hydrogenation or hydrogenolysis of the side group is linked to the presence of a methyl group in the molecule. No hydrogenation of the furan ring is detected on the intermediates.

## Introduction

Selective production of biofuels with high octane number and high energy density, such as 2,5-dimethylfuran (DMF) and 2,5-dimethyltetrahydrofuran (DMTHF), is currently highly sought for in the context of sustainable development. These two molecules derive from 5-hydroxymethylfurfural (HMF), a platform molecule produced by dehydration of hexoses.<sup>[1]</sup> HMF contains a furan ring bearing both a pending aldehyde function at the C2-position, and a hydroxymethyl group at the C5-position.<sup>[2]</sup> Transformation of HMF to DMF may go through two routes, both involving hydrogenolysis of the side-groups, either starting with the hydrogenation reaction of the aldehyde function, thus giving 2,5-bis(hydroxymethyl)furan (BHMF) as an intermediate, or with the hydrogenolysis of the hydroxyl group, giving 5-methylfurfural (MFFR) as an intermediate (Scheme 1).<sup>[3]</sup> The formation of DMTHF is usually supposed to take place in a second stage, via

DMF furan ring hydrogenation, rather than from the hydrogenolysis of hydroxymethyl tetrahydrofurans.<sup>[4]</sup> Finally, competing polymerization and ring opening reactions may also occur.

HMF being a multifunctional compound, one challenge for its upgrading is thus to increase selectivity to the valuable desired products, as several undesired reactions can occur in such a network of parallel and consecutive reactions. Catalysts based on noble metals such as Pt, Pd, and Ru have proved highly active and selective in the reductive transformation of HMF to DMF and DMTHF. For the production of DMF, a CuRu/C catalyst was first proposed, giving a yield of 76-79%.<sup>[5]</sup> The best performance was then obtained with a Pd/C catalyst under supercritical conditions, achieving a total conversion of HMF to DMF in water at 80 °C, under 100 bar CO<sub>2</sub> and 10 bar H<sub>2</sub> after 2 h. For the synthesis of DMTHF, it is a sulfur-modified Pt/C catalyst that was first proposed, giving a yield of 50%.<sup>[6]</sup> However, noble metal-based catalysts suffer from the limited availability and high cost of the metals, which may hinder their commercial applications on a large scale.<sup>[7]</sup>



**Scheme 1.** Hydrogenation of HMF to DMF and DMTHF and possible side reactions (dotted arrows represent side reactions).

Alternative solutions should be found in non-noble transition metals (e.g., Cu, Co or Ni), which are more abundant but generally less active. High yields of DMF and/or DMTHF generally require bimetallic combinations (Ni-Cu, Ni-Fe, Cu-Co, Cu-Zn, etc.), bifunctional catalysts containing both metallic and acidic active sites, and/or the use of supports that participate in the reaction directly or indirectly via their specific surface properties (TiO<sub>2</sub>, ZnO).<sup>[8,9]</sup> For example, Seemala *et al.* used TiO<sub>2</sub> as support to selectively form strong Ni-TiO<sub>2</sub> interactions in Cu-Ni/TiO<sub>2</sub>. This resulted in a deficit of Ni at the particle surface and in a promotion of the hydrogenation activity of Cu without

[a] Dr. Shuo Chen, Dr. Carmen Ciotonea, Dr. Robert Wojcieszak, Dr. Eric Marceau, Prof. Franck Dumeignil, Prof. Sebastien Royer Univ. Lille, CNRS, Centrale Lille, ENSCL, Univ. Artois, UMR 8181 - UCCS - Unité de Catalyse et Chimie du Solide, F-59000 Lille, France ; Corresponding author : [eric.marceau@univ-lille.fr](mailto:eric.marceau@univ-lille.fr); [sebastien.royer@univ-lille.fr](mailto:sebastien.royer@univ-lille.fr)

[b] Prof. Karine Vigier De Oliveira IC2MP – UMR CNRS 7285, University de Poitiers, F-86000 Poitiers, France

compromising selectivity.<sup>[10]</sup> The DMF yield was then 84% at complete conversion at 200 °C, under 2.5 bar in 1,4-dioxane after 8 h. Luo *et al.* showed that bimetallic carbon-supported NiCu<sub>3</sub> nanocrystals prepared by a solvothermal method, and consisting of a Cu-rich core and a 1:1 molar Ni:Cu shell, led to an excellent DMF yield of 99% at complete conversion at 180 °C under 33 bar in a continuous flow reactor.<sup>[11]</sup>

Since emphasis was early put on the need for an auxiliary metal or for surface acidic sites to obtain a selective catalyst, the catalytic properties of monometallic catalysts based on non-noble metals have been paradoxically less explored.<sup>[12,13]</sup> Ni-based catalysts are known for their hydrogenation ability,<sup>[14]</sup> but successes in the selective conversion of HMF have mostly been achieved with bimetallic or multifunctional catalysts, *e.g.*, Ni-W<sub>2</sub>C/C, Ni-Fe/CNTs (carbon nanotubes), Ni/LaFeO<sub>3</sub> and others.<sup>[15-18]</sup>

Kong *et al.* have published a series of papers in which the reactivity of monometallic Ni catalysts was investigated.<sup>[14,19-20]</sup> Raney Ni was shown to be active in the hydrogenation of the aldehyde function and of the furan ring of HMF to BHMTFH at 100°C in dioxane, while hydrogenation and hydrogenolysis of the side-groups to DMF was favored at a higher temperature of 180°C.<sup>[19]</sup> Unexpectedly, the hydrogenation of the furan ring was not as predominant at 180°C as it was at 100°C, with DMTHF building only slowly from DMF at that temperature. It was concluded by the authors that the methyl groups of DMF inhibited its adsorption on the Raney Ni surface. The presence of acidic groups on the catalyst surface was thus considered as critical to promote both hydrogenolysis reactions and the hydrogenation of the furan ring on Ni. In later works by the same team,<sup>[20]</sup> Lewis acidic sites were introduced through the incomplete reduction of Ni<sup>2+</sup> ions from a phyllosilicate precursor, or from an aluminic support derived from the decomposition of a hydrotalcite. The production of DMTHF was almost quantitative at 150°C in the first case, and at 180°C in the second case. In contrast, the hydrogenolysis properties of 20 and 36 Ni wt.% catalysts supported on pure silica - a support that lacks of acidic groups - and prepared by impregnation, were quite poor, even at 180°C, and a wide slate of products was obtained. Finally, DMF and DMTHF were formed in a parallel manner on the hydrotalcite-derived catalyst at 180°C, and not consecutively as would be expected, and as was indeed found on Raney Ni.<sup>[14,20]</sup>

In view of these apparent contradictions, we propose to re-examine herein the catalytic properties of the non-promoted monometallic Ni/SiO<sub>2</sub> system, by using a Ni/SBA-15 catalyst prepared by incipient wetness impregnation followed by mild drying. The SBA-15 support was chosen for its high surface area. Reaction conditions were screened for the production of DMF and DMTHF from HMF, and a kinetic profile evidencing the reaction intermediates was obtained. The results of this study not only prove that monometallic non-promoted Ni catalysts are potent systems for the selective hydroconversion of HMF to biofuel products, but also provide an understanding of the processes leading to the production both of DMF and DMTHF.

## Results and Discussion

### Catalyst characterization

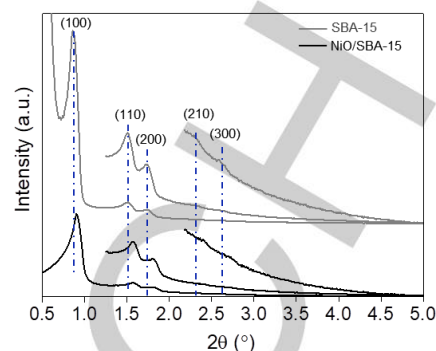


Figure 1. Low angle XRD patterns recorded for SBA-15 and NiO/SBA-15.

Figure 1 depicts the low angle X-ray diffraction domain for SBA-15 and NiO/SBA-15. Both the support and the calcined NiO/SBA-15 catalysts exhibit one intense diffraction peak and four less intense diffraction peaks, indexed to the (100), (110), (200), (210) and (300) planes: the ordered hexagonal 2D structure of *p6mm* symmetry in SBA-15 is well preserved after the formation of nickel oxide, as formerly reported.<sup>[21]</sup> The intensity decrease and the position shifts of the diffraction peaks of NiO/SBA-15 as compared to SBA-15 could be explained by the localization of NiO nanoparticles (NPs) inside the support pores. Filling of pores reduces the electron density contrast between the pores and silica walls, affecting reflections positions and their intensities.<sup>[21,22]</sup>

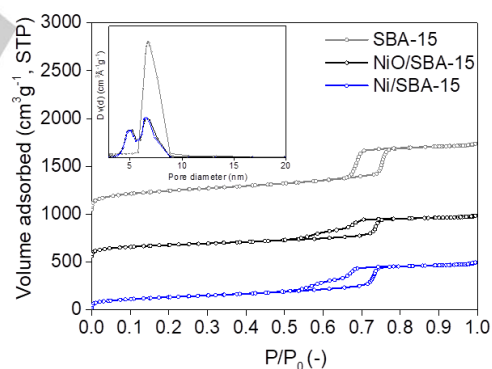


Figure 2. N<sub>2</sub> physisorption isotherms and BJH pore size distribution (inset) obtained for SBA-15, calcined NiO/SBA-15 and reduced Ni/SBA-15 catalyst (vertical shift of 500 cm<sup>3</sup>/g between isotherms for better clarity).

N<sub>2</sub> adsorption/desorption isotherms obtained for SBA-15, NiO/SBA-15 (calcined material) and Ni/SBA-15 (reduced material) are presented in Figure 2, and the calculated textural properties are listed in Table 1. An isotherm shape of Type IV according to the IUPAC classification is obtained in all cases, confirming the retaining of a well ordered mesopore structure after the impregnation step and the thermal treatments. However, the change of the hysteresis shape for the catalysts, with a two-

step desorption and a delayed closure at lower relative pressure ( $P/P_0 = 0.46$  vs.  $0.61$  for the support) is indicative of the confinement of NiO NPs in the main mesopores of SBA-15.<sup>[23]</sup> The B.J.H. pore size distribution (Figure 2, inset) shows two maxima: a first maximum located at  $6.6$  nm, close to the diameter of the primary mesopores measured for the bare SBA-15 support; a second maximum located at  $5.2$  nm which is associated to the pores filled by the NiO particles. Both open and NPs-filled cylindrical mesopores are thus present in the material. Surface area and pore volume are observed to decrease after introduction of nickel ( $>30\%$  of decrease), which is consistent with the pore plugging phenomenon and the increase in material weight density after deposition. Only a slight additional decrease in the surface area ( $-9\%$ ) and the pore volume ( $-6\%$ ) are observed after nickel reduction, while the pore size distribution remains almost unchanged.

The reducibility of NiO species was investigated by  $H_2$ -TPR (Figure 3(A)). The  $H_2$ -TPR profile of NiO/SBA-15 presents two main hydrogen consumption peaks, located at  $389^\circ\text{C}$  and  $495^\circ\text{C}$ , respectively, with a small  $H_2$  consumption also visible at  $300^\circ\text{C}$ . According to the literature, the reduction of bulk NiO generally takes place at temperatures below  $420^\circ\text{C}$ .<sup>[24]</sup> The main hydrogen consumption ( $300 - 389^\circ\text{C}$ ) is then associated to NiO NPs behaving like bulk NiO: NiO NPs confined in the mesopores or large NiO particles located at the external surface of the silica grains. Finally, the consumption observed at  $495^\circ\text{C}$  is associated to the reduction of smaller NiO particles, in stronger interaction with the silica surface. Indeed, small NiO particles are reported to be less reducible than larger particles behaving like bulk unsupported particles.<sup>[25]</sup> Quantification leads to a value of  $14.3$  mmol  $H_2/g_{\text{cat}}$ , confirming the complete reduction of Ni(II) into Ni(0).

**Table 1. Physico-chemical properties of SBA-15, NiO/SBA-15 (calcined), Ni/SBA-15 (reduced) and Ni/SBA-15-used (after reaction).**

Catalyst	$S_{\text{BET}},^{[a]}$ $\text{m}^2/\text{g}$	$V_t,^{[a]}$ $\text{cm}^3/\text{g}$	$D_p,^{[a]}$ nm	$d_{\text{Ni}},$ nm
SBA-15	841	1.10	6.8	-
NiO/SBA-15	519	0.70	5.2, 6.6	16.5 <sup>[b]</sup> , 15.9 <sup>[c]</sup>
Ni/SBA-15	468	0.66	5.2, 6.6	15.5 <sup>[b]</sup> , 14.7 <sup>[c]</sup>
Ni/SBA-15-used	242	0.50	4.9, 7.0	14.5 <sup>[b]</sup> , n.a. <sup>[d]</sup>

[a] B.E.T. surface area, total pore volume, and B.J.H. pore size obtained from  $N_2$  physisorption; [b] Average crystal size measured for NiO or Ni using the Scherrer equation; [c] Average size measured from statistical analysis on TEM images. [d] n.a.: not analysed.

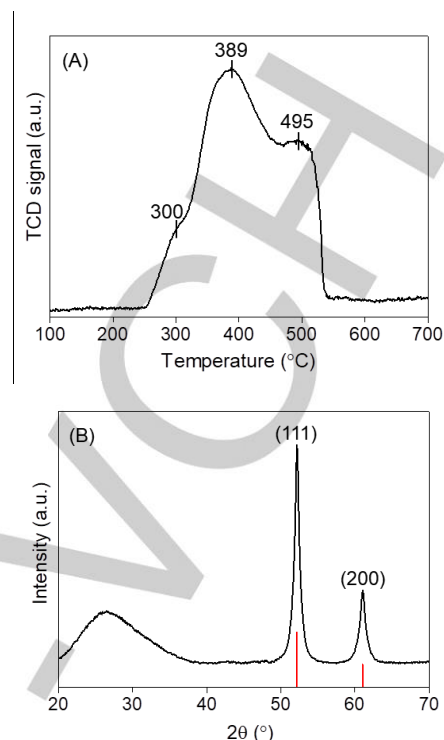


**Figure 3.** (A)  $H_2$ -TPR profile for calcined NiO/SBA-15; (B) XRD pattern of reduced Ni/SBA-15 (vertical bars: JCPDS file n° 04-0850).

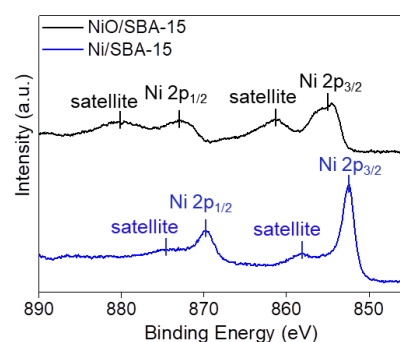


**Figure 4.** XPS high resolution spectra of the Ni 2p core levels recorded for NiO/SBA-15 and Ni/SBA-15 catalysts.

The speciation of nickel after reduction at  $550^\circ\text{C}$  for 2 h was first determined using XRD analysis (Figure 3(B)). Diffraction peaks at  $52.2^\circ$  and  $61.0^\circ$ , as well as the corresponding interplanar spacing values ( $d_{111} = 0.20$  nm,  $d_{200} = 0.18$  nm), indicate the presence of the cubic Ni(0) phase (JCPDS 04-0850). The broad onset of the otherwise narrow peaks suggests the formation of crystalline domains of both small and large sizes, with a crystal domain size, calculated by applying the Scherrer equation to the narrower part of the peaks, of  $15.5$  nm (Table 1).

XPS spectra of the Ni 2p core levels were recorded for NiO/SBA-15 and Ni/SBA-15 (Figure 4). Only  $Ni^{2+}$  species

(binding energy of 854.7 eV) are identified on the NiO/SBA-15 catalyst calcined at 550°C.<sup>[26]</sup> After reduction at 550°C, the Ni 2p<sub>3/2</sub> signal shifted to 852.5 eV, which indicates the formation of metallic Ni(0),<sup>[27]</sup> and, in line with TPR and XRD, the absence of residual oxidized nickel after reductive treatment.

The dispersion of the nickel phase in Ni/SBA-15 was further evaluated by TEM (Figure 5). After activation of the catalyst under reducing conditions, the regular hexagonal arrangement of pores was seen to be maintained, in agreement with the conclusions issued from low angle XRD. In line with N<sub>2</sub> physisorption, both empty and full mesopores exist in the structure. Two types of nickel particles are observed: in minority, large nickel particles (20-50 nm) on the external surface of the silica grains (Figure 5A); in majority, small oblong-shaped nickel NPs confined within the support channels, and having a size of ~8 nm (width) - ~15 nm (length) (Figure 5B,C). As shown in the particle size distribution (Figure 5D), most of the Ni particles belong to the 5-15 nm range, these particles being located within the main mesopores of the support. The population of external NPs with larger sizes amounts to 14% of the whole distribution.

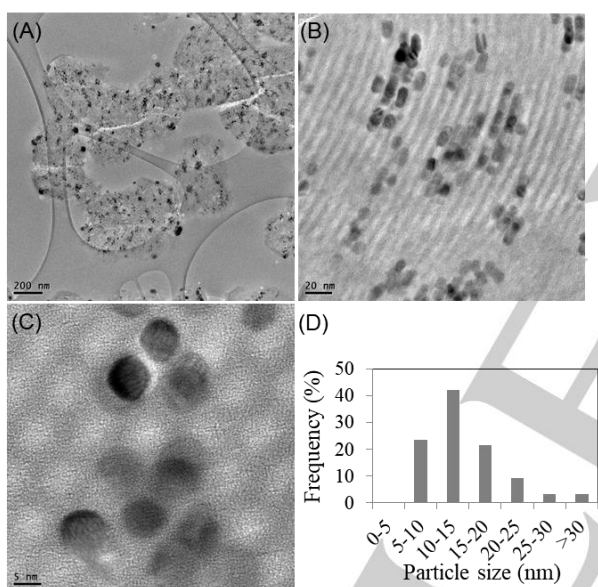


Figure 5. (A) Representative TEM images recorded for Ni/SBA-15; (B) Ni(0) particle size distribution obtained by statistical analysis of TEM images.

### Catalytic properties

Dioxane was chosen as the solvent, considering its stability in reaction, the solubility of HMF in this solvent, the better yields to the target products than when other solvents are used,<sup>[10]</sup> and the possibility of comparison with the results from Kong *et al.*<sup>[19]</sup> In order to determine which reaction parameters would lead to high DMF/DMTHF yields over Ni/SBA-15, a L9 set of orthogonal experiments (3 (levels) ^ 3 (factors)) was constructed according to the Taguchi method using software Minitab 17. Three process parameters (*i.e.*, reaction temperature, H<sub>2</sub> pressure and HMF/Ni molar ratio) were selected on the basis of the available literature.<sup>[28]</sup> When the temperature is lower than 180°C, the

hydrogenolysis of the C-O bond (the reaction affording DMF/DMTHF) has been reported to become slow.<sup>[19]</sup> On the other hand, the selectivity to DMF/DMTHF generally decreases above 240°C, owing to the formation of by-products such as humins.<sup>[10,29]</sup> Hence, the reaction temperature was set in the range of 180-240°C. As maximum DMF/DMTHF yields were obtained below 50 bar of hydrogen,<sup>[1]</sup> 45 bar was selected as the maximum pressure level. The hydrogen pressure was thus chosen in the range 15-45 bar, considering that increasing hydrogen pressure increases the concentration of hydrogen in the solvent, which may benefit to the conversion rate. Finally, the HMF/Ni molar ratio was varied in the range of 3-30 at constant concentration of HMF, covering the range of the HMF/Ni molar ratios mentioned in the literature.<sup>[1]</sup>

Table 2. Conversions and product distributions obtained under screening conditions<sup>[a]</sup>

No.	T /°C	P /bar	HMF/Ni mol. ratio	conv. /%	yield/%				C.B. /% <sup>[b]</sup>
					DMF	DMT HF	MFF R	MF OL	
1	180	15	30	7	1	0	1	2	97
2	180	30	3	100	1	81	1	1	85
3	180	45	15	34	12	0	2	10	90
4	210	15	3	100	1	72	1	1	76
5	210	30	15	44	41	1	2	0	100
6	210	45	30	21	17	1	1	2	100
7	240	15	15	32	21	3	8	0	100
8	240	30	30	11	7	1	1	2	100
9	240	45	3	100	0	55	1	1	58

[a] Catalytic tests were performed in batch-pressurized reactors, using an Autoplant-Chemspeed instrument, with 0.15 mmol/mL HMF in 25 mL 1,4-dioxane solution for 8 h. [b] Carbon balance.

Reaction parameters, HMF conversion, main products' yields and carbon balances are summarized in Table 2. The parameters screening showed that:

- (1) DMF and DMTHF were the major products, but MFFR and MFOL were also detected after 8 h of reaction. These results indicate that the hydrogenolysis of the C-OH bond and the furan ring hydrogenation are favored over the Ni/SBA-15 catalyst;
- (2) low HMF/Ni molar ratios ( $\leq 15$ ) or large catalyst quantity ( $\geq 0.052$  g) are required for an efficient conversion of HMF;
- (3) hydrogen pressure in the selected range (15-45 bar) has a weaker influence on the catalytic results than the HMF/Ni molar ratio and the reaction temperature;
- (4) lower carbon balances (decreasing down to 58%) are obtained when the HMF/Ni molar ratio decreases, an effect more visible at high reaction temperatures (Table 2, Entry 4 and 9), due to possible polymerization reaction with BHMF and MFOL.<sup>[30]</sup>

Two of these nine tests stand out. In Entry 5, a DMF yield of 40.6% at 43.8% HMF conversion was obtained at 210°C under 30 bar H<sub>2</sub> with a HMF/Ni molar ratio of 15, giving a maximum DMF selectivity (93%). However, the conversion of HMF is limited under these reaction conditions and duration because of

the low catalyst loading. In Entry 2, a DMTHF yield of 81.4% (100% HMF conversion) was obtained at 180 °C under 30 bar H<sub>2</sub> with a HMF/Ni molar ratio of 3, suggesting that these conditions are suitable for the selective production of DMTHF over Ni/SBA-15: DMTHF yield and carbon balance decrease at 210°C (Entry 4). This result is quite interesting considering that only one report in the literature reported similarly high DMTHF yield obtained with Ni-based catalysts.<sup>[28]</sup> It can be wondered if the DMF yield can also be high under these reaction conditions, according to the HMF → DMF → DMTHF pathway depicted in Scheme 1.

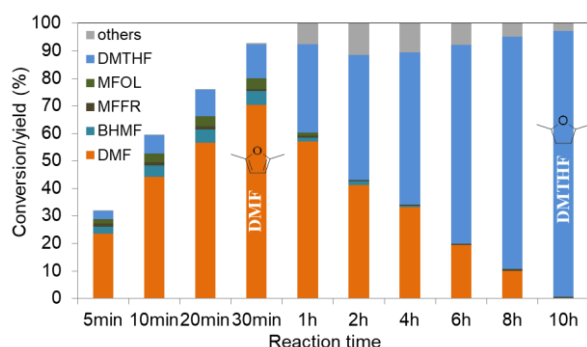


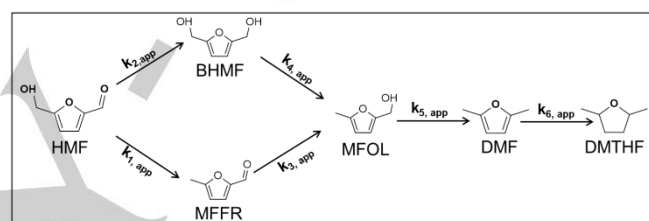
**Figure 6.** Evolution of HMF conversion and product yields with reaction time over Ni/SBA-15. Reaction conditions: 0.144 mmol/mL HMF in 25 mL 1,4-dioxane, P(H<sub>2</sub>) = 30 bar, T = 180°C, HMF/Ni molar ratio of 3.

The evolution of HMF conversion and products yields in these reaction conditions (180°C, 30 bar H<sub>2</sub>, HMF/Ni molar ratio of 3) was next followed as a function of reaction time (Figure 6). At short reaction time (30 min), HMF was primarily and rapidly converted into DMF (70.5% yield), and the yield of DMTHF was limited (12.2% yield). BHMf and MFOL were also detected at low concentrations (4.9 and 4.0% yields, respectively), indicating the existence of a hydrogenation-hydrogenolysis pathway to DMF (Scheme 1). Only a low amount of MFFR, the intermediate in the hydrogenolysis-hydrogenation pathway, was comparatively detected (0.8% yield). The DMF yield obtained after 30 min is quite comparable to the results obtained over monometallic Ni-based catalysts reported in the literature (Table 3), especially considering that most catalytic performances have relied on the use of supports bearing other chemical functions (Entries 4-5). The results reported in the present work then show that, in contradiction with former results obtained on Ni/SiO<sub>2</sub> catalysts in similar conditions [28], a non-promoted monometallic Ni catalyst can afford a high hydrogenolysis ability to form a major amount of DMF under adequate reaction conditions, even when the support presents no specific chemical function and, in particular, no acidity.

Prolonging the reaction time to 1 h led to complete HMF conversion, with a significant decrease of the DMF yield (57.0%) at the expense of the DMTHF yield (32.1%). The concentrations of BHMf and MFOL also decreased to negligible levels (yields <2%). During this period, the main reaction occurring is the furan ring hydrogenation of DMF to DMTHF, appearing in a sequential

way. When the reaction time was prolonged above 1 h, the yield of DMTHF continuously increased, reaching 96.6% at complete HMF conversion after 10 h. The DMF yield was negligible after 10 h (0.6%).

In summary, HMF was first and rapidly converted into DMF by hydrogenolysis, BHMf, MFFR and MFOL being intermediates products detected. The furan ring hydrogenation of DMF to DMTHF occurred in a second stage, at a slower rate, explaining the need for a longer reaction time to maximize its yield. As compared to the reports available in the literature (Table 3, Entries 8-11), the DMTHF yield obtained in this work is among the highest reported. Only Kong et al. reported comparable results, but using a bifunctional Ni/Al<sub>2</sub>O<sub>3</sub> catalyst derived from a hydrotalcite-like precursor (Table 3, Entry 11), after 20 h of reaction at 180°C under 12 bar and with a higher HMF/Ni molar ratio of 11.<sup>[20]</sup> The parallel productions of DMF and DMTHF in their work let one suppose that sites presenting different types of reactivity were active on this catalyst.



**Scheme 2.** Kinetic scheme proposed for the DMTHF production from HMF (k<sub>app</sub>: apparent rate constant)

### Kinetics of the reaction

Based on these measurements, it was attempted to build a simplified kinetic model to describe the catalyst properties, lying on the hypotheses described in the Supporting Information file. The transformation of HMF to DMF and DMTHF supposes the formation of MFOL as intermediate (Scheme 2). MFOL itself can be produced following two routes:

- (1) Hydrogenolysis of HMF to MFFR, followed by the hydrogenation of the aldehyde function of MFFR to MFOL.
- (2) Hydrogenation of the aldehyde function of HMF to BHMf, followed by the hydrogenolysis of BHMf to MFOL.

When reaction is performed at 180°C, both MFFR and BHMf are detected in small amounts at short reaction times. As will be seen below, MFOL appears in parallel to BHMf, and not in a second stage as would be the case if it was produced from BHMf only. It is thus not possible to eliminate one of these two routes a priori. Furthermore, as DMTHF appears in the last stage, once DMF has been produced and accumulated, and other hydrogenation products have not been detected, we will suppose that the hydrogenation of the furan ring does not take place to a large extent on the minor intermediate products.<sup>[31]</sup> A fitting of the apparent rate constants was performed by least-square minimization, according to a mechanism based on the following steps:<sup>[31,32]</sup>

- HMF being consumed by paths 1 and 2, its consumption was fitted using a first-rate law of rate constant ( $k_{1,app} + k_{2,app}$ ):

$$[HMF] = [HMF]_0 \exp(-((k_{1,app} + k_{2,app})t)) \quad (1)$$

- As a primary intermediate product, MFFR neat production rate was defined as the difference between the production rate  $k_{1,app}$  [HMF] and the consumption rate  $k_{3,app}$  [MFFR], leading to Eq. (2):

$$[MFFR] = \frac{k_{1,app}[HMF]_0}{k_{3,app} - (k_{1,app} + k_{2,app})} [\exp(-k_{1,app}t) - \exp(-k_{3,app}t)] \quad (2)$$

**Table 3. Catalytic performances of Ni-based catalysts for the conversion of HMF to DMF and DMTHF.**

No.	Catalyst	Feed conditions	P (bar)	T (°C)	t (h)	X (%)	Y (%)	ref
<b>HMF to DMF</b>								
1	Raney Ni	12 mmol HMF; 35 mL 1,4-dioxane; 0.5 g catalyst	15	180	15	100	89	[19]
2	Ni/Ni <sup>2+</sup> -silicate <sup>[a]</sup>	12 mmol HMF; 38 mL 1,4-dioxane; 0.08 g catalyst	15	130	3	100	73	[14]
3	Ni/CN <sup>[b]</sup>	2 mmol HMF; 20 mL water; 0.05 g catalyst	30	200	6	100	99	[13]
4	Ni/LaFeO <sub>3</sub>	1 mmol HMF; 12 mL ethanol; 0.1 g catalyst	50	230	6	99	98	[17]
5	Ni/C	8 mmol HMF; 100 mL 1-propanol; W/F = 2 g <sub>min</sub> /mL	33	180	-	92	53	[12]
6	Ni/Al <sub>2</sub> O <sub>3</sub>	12 mmol HMF, 35 mL 1,4-dioxane, 0.1 g catalyst	12	180	4	100	92	[20]
7	Ni/SBA-15	1.8 mmol HMF; 12.5 mL 1,4-dioxane; 0.261 g catalyst	30	180	0.5	93	71	<b>this work</b>
<b>HMF to DMTHF</b>								
8	Pd/C	8 mmol HMF, 100 mL 1-propanol	33	180	-	100	55	[12]
9	CuZn	4 mmol HMF, 20 mL CPME, 0.1 g catalyst	20	220	6	100	25	[9]
10	Ni/SiO <sub>2</sub>	12 mmol HMF, 38 mL 1,4-dioxane, 0.08 g catalyst	15	150	3	100	26	[14]
11	Ni/Al <sub>2</sub> O <sub>3</sub>	12 mmol HMF, 35 mL 1,4-dioxane, 0.1 g catalyst	12	180	20	100	97	[20]
12	Ni/SBA-15	1.8 mmol HMF; 12.5 mL 1,4-dioxane; 0.261 g catalyst	30	180	10	100	97	<b>this work</b>

[a] Ni(0)/Ni(+II) catalyst from nickel phyllosilicate; [b]: Ni/CN, Ni supported on mesoporous nitrogen-rich carbon.

- As a primary intermediate product, BHMF neat production rate was defined as the difference between the production rate  $k_{2,app}$  [HMF] and the consumption rate  $k_{4,app}$  [BHMF], leading to Eq. (3):

$$[BHMF] = \frac{k_{2,app}[HMF]_0}{k_{4,app} - (k_{1,app} + k_{2,app})} [\exp(-k_{1,app}t) - \exp(-k_{4,app}t)] \quad (3)$$

A first fitting of HMF consumption, and of MFFR and BHMF neat productions, led to the first evaluation of the four first apparent rate constants,  $k_{1,app}$  to  $k_{4,app}$ , and to the calculation of  $r_1$  to  $r_4$ . It appeared that  $r_1$  was approximately 10 times higher than  $r_2$ , and that  $r_3$  was larger than  $r_4$  by a factor of 20 to 40. The main production path to MFOL was thus identified as the one involving MFFR (Scheme 3).

- The neat production of the secondary intermediate, MFOL, was then based on the HMF → MFFR → MFOL pathway, of rate constants  $k_{1,app}$  and  $k_{3,app}$ , for the production side, and  $k_{5,app}$  for the consumption rate (Eq. 4):

$$[MFOL] = (k_{1,app} k_{3,app}) [HMF]_0 \left[ \frac{\exp(-k_{1,app}t)}{(k_{3,app} - k_{1,app})(k_{5,app} - k_{1,app})} - \frac{\exp(-k_{3,app}t)}{(k_{1,app} - k_{3,app})(k_{5,app} - k_{3,app})} + \frac{\exp(-k_{5,app}t)}{(k_{1,app} - k_{5,app})(k_{3,app} - k_{5,app})} \right] \quad (4)$$

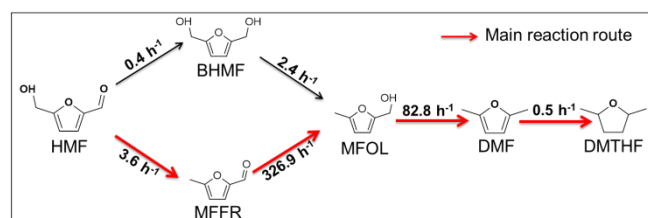
allowing the fitting of constant  $k_{5,app}$  along with  $k_{1,app}$  -  $k_{4,app}$ .

- As DMF is not the final product of reaction, it is not possible to model its production just by subtracting the concentrations of HMF, BHMF, MFFR and MFOL from [HMF]<sub>0</sub>. However, BHMF, MFFR and MFOL being formed in very low amounts with respect to DMF and DMTHF, it can be attempted to apply the steady state approximation to these intermediates, and consider that the production rate of DMF is close to the consumption rate of HMF. DMF thus becomes an intermediate between HMF and DMTHF, and its concentration follows the law:

$$[DMF] = \frac{(k_{1,app} + k_{2,app})[HMF]_0}{k_{6,app} - (k_{1,app} + k_{2,app})} [\exp(-k_{1,app}t) - \exp(-k_{6,app}t)] \quad (5)$$

making it possible to fit  $k_{6,app}$  with the other constants.

(6) Finally, DMTHF is calculated as the difference between [HMF]<sub>0</sub>, and the concentrations of all the other products, including the unknown ones completing the carbon balance at 100% (which implicitly supposes that these unknown products derive from the last stages of the global reaction and not from the consumption of intermediates).



**Scheme 3.** Apparent rate constants for each reaction step of HMF conversion to DMTHF

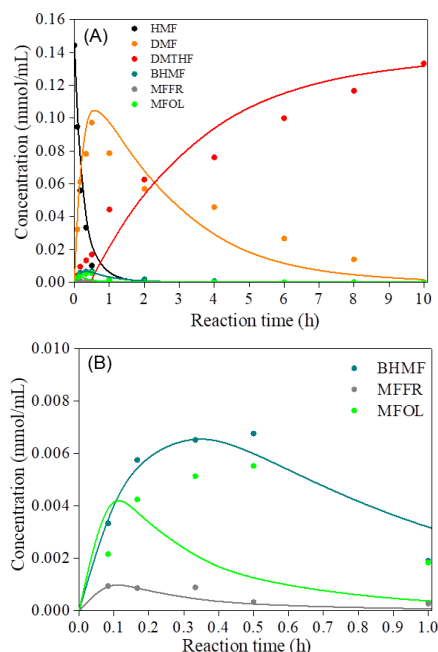


**Figure 7.** Kinetic patterns of HMF conversion over Ni/SBA-15 simulated after least-square minimization of the apparent rate constants (A); enlargement of the kinetic patterns during the first hour (B). Reaction conditions: 0.144 mmol/mL HMF in 12.5 mL 1,4-dioxane,  $P(\text{H}_2) = 30$  bar,  $T = 180^\circ\text{C}$ , HMF/Ni molar ratio of 3, data points and solid lines represent experimental data and model, respectively.

The values of the six apparent rate constants found after least-square minimization are presented in Scheme 3. A graphical comparison between the experimental and the modelled concentrations (Figure 7) raises the following comments:

(1) HMF consumption, MFFR production and BHMf production are correctly modelled, in particular the position of the maximum of production of MFFR and BHMf.

(2) In contrast, the production of MFOL is poorly reproduced, as its consumption starts too early. Decreasing  $k_{5,\text{app}}$  shifts the maximum of production to longer times, but also increases considerably the amount of MFOL formed, which means that  $k_{3,\text{app}}$  would also need to be better adjusted. There is thus an uncertainty on the values of  $k_{3,\text{app}}$  and  $k_{5,\text{app}}$  obtained by this model. A new fitting based only on the concentrations of the minor species led to a decrease of the two rate constants, but at the expense of the quality of the fitting for BHMf. In any case,  $k_{3,\text{app}}$  and  $k_{5,\text{app}}$  were still large compared to  $k_{2,\text{app}}$  and  $k_{4,\text{app}}$ .

(3) The fits for DMF and DMTHF follow the same tendency as the experimental data, though at longer times the consumption of DMF and the production of DMTHF are overestimated. Some inhibition phenomena not taken into account here can be postulated.

In summary, on the tested Ni catalyst, both C=O hydrogenation and hydrogenolysis steps are fast compared to the hydrogenation of the furan ring. C-O hydrogenolysis and C=O hydrogenation reactions are in competition. The MFFR route seems to be predominant, confirming the capability of the Ni

catalyst for the hydrogenolysis reaction. The apparent rate constants of the hydrogenation and hydrogenolysis steps involving intermediates containing a methyl group (MFFR, MFOL) are found to be much larger than in the others steps, suggesting a fast adsorption/reaction of these molecules on the catalyst surface. However, one should recall that the model built here is very simple and perhaps too simplified, and uncertainties remain large concerning these intermediates, which one should remember are detected in quite low amounts at very short reaction times.

### Stability of Ni/SBA-15

The recyclability of the SBA-15 supported Ni catalyst was finally evaluated (Figure 8). Between each reaction cycle, the catalyst was recovered by centrifugation and washed with acetone. The catalyst was re-calcined at  $500^\circ\text{C}$  for 6 h and re-reduced at  $550^\circ\text{C}$  for 2 h before the next test in order to avoid the presence of Ni oxidized species that can negatively affect the activity. Each test was performed for 3 h at  $180^\circ\text{C}$  under 30 bar  $\text{H}_2$ . In the first run, the HMF conversion was 100% with a DMF yield of 45% and a DMTHF yield of 48% (Figure 8). After 3 cycles, the HMF conversion had decreased to 75%, with an increasing amount of unreacted BHMf, while the DMF yield and DMTHF yield had been reduced to 37 and 10%, respectively. Progressive deactivation is thus a source of concern for this nickel catalyst.

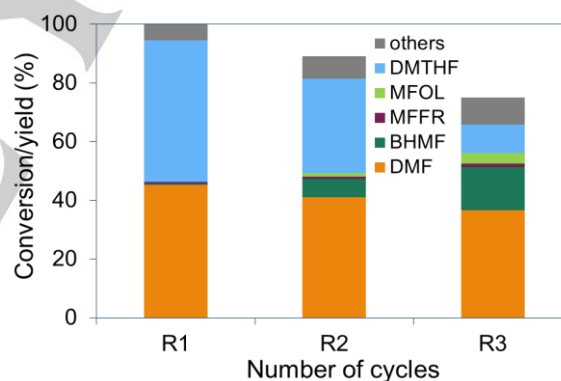


**Figure 8.** Recyclability of the Ni/SBA-15 catalyst for the HMF hydrogenation reaction. Reaction conditions: 0.15 mmol/mL HMF in 20 mL 1,4-dioxane,  $P(\text{H}_2) = 30$  bar,  $T = 180^\circ\text{C}$ , HMF/Ni molar ratio of 3, 3 h.

After the reaction, the spent catalyst was analyzed by XRD, TEM, IR spectroscopy and C-content analysis, and the Ni content in the reaction solution was analyzed by ICP in order to identify the main cause of the catalyst deactivation. No increase of the Ni crystal size was measured applying the Scherrer equation to the XRD pattern (Table 1). The absence of significant sintering and mesostructured degradation during reaction was confirmed by microscopy (Figure 9A-F). The majority of the particles were again found to be confined in the well-defined mesopores of SBA-15, with a few aggregated Ni particles outside the channels (Figure 9A,B). Besides, according to the ICP analysis, the Ni content in the reaction solution after the recycling tests is of 1.53 ppm. Considering the quantity of Ni

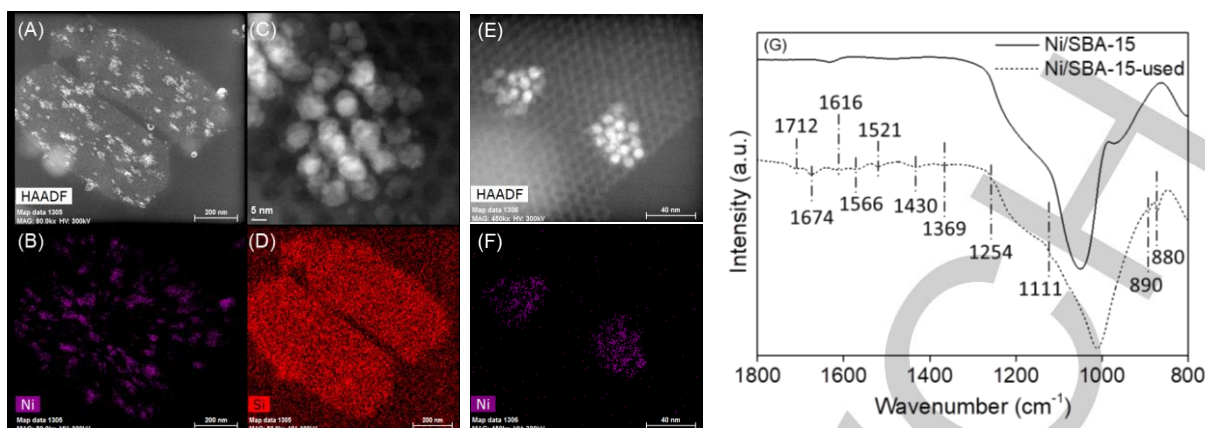


**Figure 9.** HRTEM HAADF images (A,C,E) and Ni (B,F) and Si (D) mapping of the Ni/SBA-15-used sample; (G) FT-IR spectra of the fresh and used Ni/SBA-15 catalysts.

from the catalyst presents in the reactor, it corresponds to 0.055 wt.% of the total Ni content. Such result is indicating that the Ni leaching is negligible, as it could be awaited considering that the reaction is performed in organic solvent. Consequently, the deactivation is not associated to modifications of the support characteristics, Ni dispersion change or Ni leaching. Another possible way of deactivation is the adsorption of high molecular weight compounds on the active sites during the reaction.<sup>[33]</sup> The FT-IR spectrum, shown in Figure 9E for the used catalyst, exhibits bands at:

- 880  $\text{cm}^{-1}$  (adsorption of furan compounds)<sup>[34]</sup>
- 890 and 1254  $\text{cm}^{-1}$  (vibrations involving the C-H groups)<sup>[35]</sup>
- 1111, 1369 and 1430  $\text{cm}^{-1}$  (C-O stretching vibration)<sup>[36]</sup>
- 1521, 1566, 1616, 1674 and 1712  $\text{cm}^{-1}$  (assigned to C=O groups)<sup>[36]</sup>

These results, added to C-content analysis results demonstrating a 9.2 wt.% carbon content in the used catalyst, after the three cycles of reaction, indicate that the adsorption of organic compounds on the catalyst surface,<sup>[37]</sup> that are not efficiently removed by oxidative regeneration at 500°C, is the main reason behind the progressive deactivation during recycling tests.

## Conclusions

A non-promoted, monometallic Ni/SBA-15 catalyst prepared by incipient wetness impregnation appears to be an active system for the hydroconversion of 5-hydroxymethylfurfural (HMF) to 2,5-dimethylfuran (DMF) and 2,5-dimethyltetrahydrofuran (DMTHF). High yields of DMF and DMTHF are achieved in dioxane at 180°C under 30 bar  $\text{H}_2$ , 70.5% and 96.6% respectively, by simply modifying the reaction time. Despite the absence of acidic sites, the catalyst exhibits both a high hydrogenolysis ability and a high ability for the furan ring hydrogenation. The kinetic study suggests that HMF is converted *via* the route involving MFFR as an intermediate product. Competitive reactions of C-O hydrogenolysis and C=O hydrogenation are in

any case faster than the furan ring hydrogenation, which is the reason behind the high yields of DMF as an intermediate product toward DMTHF. The stability upon recycling of a non-promoted Ni catalyst can however be questioned, as deactivation seems to occur because of carbon deposition, rather than because of Ni nanoparticles sintering.

## Experimental Section

### Synthesis of Ni/SBA-15 catalyst

The SBA-15 support was synthesized according to a classical procedure.<sup>[38]</sup> In a typical synthesis, 4.0 g of Pluronic P123 was dissolved in a 1.6 M solution of HCl at 40 °C. Thereafter, 8.5 g of TEOS were added dropwise to the solution, and this solution was submitted to magnetic stirring for 24 h. The resulting gel was submitted for 48 h to hydrothermal ageing at 100 °C. After recovery by filtration, the SBA-15 sample was washed with water, and dried at 100 °C for 24 h. The dried SBA-15 sample was calcined at 550 °C for 6 h in a muffle furnace, using a heating ramp of 1.5 °C  $\text{min}^{-1}$ .

The nickel catalyst was prepared using the incipient wetness impregnation – mild drying method.<sup>[21]</sup> To prepare 10 g of 15 wt.% Ni/SBA-15 catalyst, 9.4 mL of an aqueous solution of nickel nitrate (2.8 mmol/mL;  $\text{Ni}(\text{NO}_3)_2 \cdot 6\text{H}_2\text{O}$ , 98% purity, Sigma-Aldrich) was dropped onto 8.5 g of SBA-15 powder (pore volume = 1.1 mL/g). The wet mixture was placed in an oven set at 25 °C and aged under static conditions for five days. A calcination under static air was finally performed at 500 °C for 6 h with a ramp of 1.5 °C/min. The calcined sample is denoted NiO/SBA-15, the reduced sample is denoted Ni/SBA-15 and the spent catalyst is denoted Ni/SBA-15-used.

### Characterization

X-ray diffraction patterns were recorded on a Bruker D8 Advance X-ray diffractometer in Bragg-Brentano configuration, with a Cu K $\alpha$  radiation ( $\lambda = 1.54184 \text{ \AA}$ ).  $\text{N}_2$  physisorption experiments were performed at -196 °C, on a Micromeritics Tristar II Plus instrument. The particle size and shape were analysed by transmission electron microscopy. For fresh catalysts, experiments were conducted on a JEOL 2100 UHR, operated at 200 kV

with a LaB<sub>6</sub> source and equipped with a Gatan 832 CCD camera. For the used catalyst, experiment was conducted on a TITAN Themis 300 S/TEM. The high angle annular dark field (HAADF) images were collected at angles between 50 and 200 mrad. Ni content in the reaction solution after recycling tests was evaluated by inductively coupled plasma optical emission spectrometry (ICP-OES) over an ICP-OES spectrometer (720-ES Agilent) with an axially viewing and a simultaneous CCD detection. H<sub>2</sub>-temperature programmed reduction (TPR) was performed on an Autochem analyzer (Micromeritics) equipped with a quartz U-shaped microreactor. Quantification of H<sub>2</sub> consumed is performed using a TCD after trapping of the produced water. The FT-IR spectra were recorded on an infrared spectrometer in the attenuated total reflectance mode (IR-ATR) from Thermo Scientific (IS50). Thermogravimetry experiments were conducted on a system from Mettler Toledo (TGA/SDTA 851 model). The experiment was conducted under 20%O<sub>2</sub> in N<sub>2</sub> flow at the rate of 50 mL/min, with a temperature increase from 50 to 900°C at a rate of 5 °C/min. X-ray photoelectron spectroscopy analyses were performed on a AXIS Ultra DLD Kratos spectrometer equipped with a monochromatized aluminium source (Al Kα = 1486.7 eV) and a charge compensation gun. The spectra were obtained after the samples were purged at room temperature under vacuum. The data were collected at a step length of 0.1 eV. For the Ni/SBA-15 catalyst, the sample was in situ reduced at 550°C for 2 h before XPS analysis.

### Hydroconversion of 5-Hydroxymethylfurfural

Preliminary catalytic tests were performed in an 8-parallel automated autoclave system equipped with 8 high-pressure batch reactors (100 mL). Prior to the catalytic tests, the catalysts were reduced at 550 °C for 2 h (heating ramp of 10 °C/min) under 5 vol.% H<sub>2</sub> in Ar flow (50 mL/min). The reactor was loaded under inert atmosphere (glove box) with 0.15 mmol/mL HMF in 25 mL 1,4-dioxane as a solvent and 0.16 g of catalyst, sealed and purged with H<sub>2</sub>. Then, the reactor was pressurized with the required H<sub>2</sub> pressure (15–45 bar), heated at the required temperature (180–240 °C) and stirred at a speed of 700 rpm for 8h. The kinetics of the reaction was followed using a 45 mL Parr reactor. The pre-reduced catalyst (550°C, 2 h, pure H<sub>2</sub> flow) was inserted in the reactor together with 12.5 mL of 0.15 mmol/mL HMF solution in 1,4-dioxane. The reactor was closed, purged with hydrogen several times, and pressurized with H<sub>2</sub> up to 30 bar at 180 °C. The pressure was monitored using a gauge connected to the reactor. The reaction was stirred magnetically. Samples of reaction medium were collected at selected reaction times: 5 min, 10 min, 20 min, 30 min, 1 h, 2 h, 4 h, 6 h, 8 h and 10 h. For each selected time, the reactor was placed into ice water for rapid cooling and the pressure was released. After the sample collection, the reactor was put back for the reaction at next reaction time and these steps were repeated until the reaction time of 10 h. The catalyst is recovered by filtration and the products were analysed by GC (Shimadzu 2010 Plus) equipped with a ZB-WAX Plus capillary column (30.0 m × 0.25 mm × 0.25 μm) and a flame ionization detector (FID), and by GC-MS (Shimadzu QP2010 Ultra EI) equipped with a ZB-1XT capillary column (15.0 m × 0.53 mm × 0.25 μm) and an FID detector.

### Acknowledgements

Chevreur Institute (FR 2638), Ministère de l'Enseignement Supérieur et de la Recherche and Région Hauts-de-France are also acknowledged for supporting this work. This work has benefited from the support of the CSC PhD scholarship program (S. C.) and of the French National Research Agency (ANR), through the NobleFreeCat project (ANR-17-CE07-0022). The

authors thank technical support from the Lille University: Martine Trentesaux and Pardis Simon for XPS analysis, Olivier Gardoll for physical and redox characterization, Laurence Burylo for XRD experiment, Maya Marinova for HRTEM analysis and Svetlana Heyte from the REALCAT platform for high throughput catalytic tests. Stéphane Pronier, from University of Poitiers, is acknowledged for TEM analysis over fresh catalyst. The REALCAT platform is benefiting from a state subsidy administrated by the French National Research Agency (ANR) within the frame of the 'Future Investments' program (PIA), with the contractual reference 'ANR-11-EQPX-0037'.

**Keywords:** HMF • hydroconversion • nickel • biofuels • incipient wetness impregnation

- [1] S. Chen, R. Wojcieszak, F. Dumeignil, E. Marceau, S. Royer, *Chem. Rev.* **2018**, 118, 11023–11117.
- [2] R. J. van Putten, J. C. van der Waal, E. de Jong, C. B. Rasrendra, H. J. Heeres, J. G. de Vries, *Chem. Rev.* **2013**, 113, 1499–1597.
- [3] a) P. Gallezot, *Chem. Soc. Rev.* **2012**, 41, 1538–1558; b) J. P. Lange, E. Van der Heide, J. Van Buijtenen, R. Price, *ChemSusChem.* **2012**, 5, 150–166; c) G. Dautzenberg, M. Gerhardt, B. Kamm, *Holzforschung.* **2011**, 65, 439–451.
- [4] T. S. Hansen, K. Barta, P. T. Anastas, P. C. Ford, A. Riisager, *Green Chem.* **2012**, 14, 2457–2461.
- [5] Y. Román-Leshkov, C. J. Barrett, Z. Y. Liu, J. A. Dumesic, *Nature.* **2007**, 447, 982–985.
- [6] M. A. Jackson, M. Appell, J. A. Blackburn, *Ind. Eng. Chem. Res.* **2015**, 54, 7059–7066.
- [7] a) J. Luo, H. Yun, A.V. Mironenko, K. Goulas, J. D. Lee, M. Monai, C. Wang, V. Vorotnikov, C. B. Murray, D. G. Vlachos, P. Fornasiero, R. J. Gorte, *ACS Catal.* **2016**, 4095–4104; b) L. Hu, X. Tang, J. Xu, Z. Wu, L. Lin, S. Liu, *Ind. Eng. Chem. Res.* **2014**, 53, 3056–3064; c) Q. Li, P. Man, L. Yuan, P. Zhang, Y. Li, S. Ai, *Molecular Catalysis.* **2017**, 431, 32–38; d) S. Nishimura, N. Ikeda, K. Ebitani, *Catal. Today.* **2014**, 232, 89–98; e) M. Chatterjee, T. Ishizaka, H. Kawanami, *Green Chem.* **2014**, 16, 1543–1551; f) J. Luo, J.D. Lee, H. Yun, C. Wang, M. Monai, C. B. Murray, P. Fornasiero, R. J. Gorte, *Appl. Catal. B.* **2016**, 199, 439–446.
- [8] a) B. Chen, F. Li, Z. Huang, G. Yuan, *Appl. Catal. B-Environ.* **2017**, 200, 192–199; b) W. Guo, H. Liu, S. Zhang, H. Han, H. Liu, T. Jiang, B. Han, T. Wu, *Green Chem.* **2016**, 18, 6222–6228; c) Y. Zhu, X. Kong, H. Zheng, G. Ding, Y. Zhu, Y.-W. Li, *Catal. Sci. Technol.* **2015**, 5, 4208–4217; d) S. Srivastava, G.C. Jadeja, J. Parikh, *J Mol Catal A-Chem.* **2017**, 426, 244–256; e) A.J. Kumalputri, G. Bottari, P.M. Erne, H.J. Heeres, K. Barta, *ChemSusChem.* **2014**, 7, 2266–2275; f) X. Kong, Y. Zhu, H. Zheng, Y. Zhu, Z. Fang, *ACS Sustain. Chem. Eng.* **2017**, 5, 11280–11289.
- [9] G. Bottari, A. J. Kumalputri, K.K. Krawczyk, B. L. Feringa, H. J. Heeres, K. Barta, *ChemSusChem.* **2015**, 8, 1323–1327.
- [10] B. Seemala, C. M. Cai, C. E. Wyman, P. Christopher, *ACS Catal.* **2017**, 4070–4082.
- [11] J. Luo, M. Monai, C. Wang, J. D. Lee, T. Duchoň, F. Dvořák, V. Matolín, C. B. Murray, P. Fornasiero, R.J. Gorte, *Catal. Sci. Technol.* **2017**, 7, 1735–1743.
- [12] J. Luo, L. Arroyo-Ramírez, J. Wei, H. Yun, C.B. Murray, R. J. Gorte, *Appl Catal A-Gen.* **2015**, 508, 86–93.
- [13] R. Goyal, B. Sarkar, A. Bag, N. Siddiqui, D. Dumbre, N. Lucas, S.K. Bhargava, A. Bordoloi, *J. Catal.* **2016**, 340, 248–260.
- [14] X. Kong, Y. Zhu, H. Zheng, X. Li, Y. Zhu, Y.-W. Li, *ACS Catal.* **2015**, 5, 5914–5920.
- [15] P. Yang, Q. Xia, X. Liu, Y. Wang, *Fuel.* **2017**, 187, 159–166.
- [16] Y. B. Huang, M. Y. Chen, L. Yan, Q.-X. Guo, Y. Fu, *ChemSusChem.* **2014**, 7, 1068–1072.
- [17] M. Y. Chen, C. B. Chen, B. Zada, Y. Fu, *Green Chem.* **2016**, 18, 3858–3866.
- [18] P. Yang, Q. Xia, X. Liu, Y. Wang, *J. Energy Chem.* **2016**, 25, 1015–1020.
- [19] X. Kong, Y. Zhu, H. Zheng, F. Dong, Y. Zhu, Y. W. Li, *RSC Adv.* **2014**, 4, 60467–60472.
- [20] X. Kong, R. Zheng, Y. Zhu, G. Ding, Y. Zhu, Y. W. Li, *Green Chem.* **2015**, 17, 2504–2514.
- [21] A. Ungureanu, B. Dragoi, A. Chiriac, S. Royer, D. Duprez, E. Dumitriu, *J. Mater. Chem.* **2011**, 21, 12529–12541.

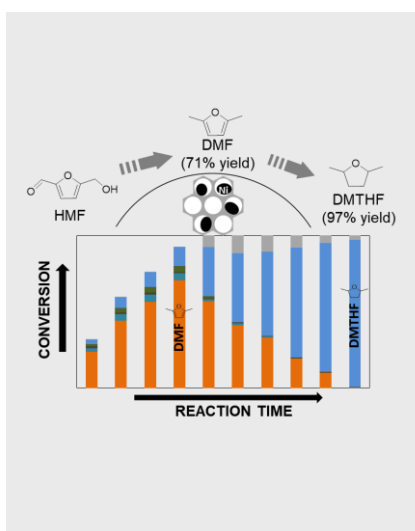
- [22] S. Chen, C. Ciotonea, A. Ungureanu, E. Dumitriu, C. Catrinescu, R. Wojcieszak, F. Dumeignil, S. Royer, *Catal. Today* **2019**, 334, 48–58.
- [23] a) J. P. Thielemann, F. Girgsdies, R. Schlögl, C. Hess, *Beilstein J Nanotech.* **2011**, 2, 110–8; b) P.V.D. Voort, P.I. Ravikovitch, K.P.D. Jong, A.V. Neimark, A.H. Janssen, M. Benjelloun, E.V. Bavel, P. Cool, B.M. Weckhuysen, E.F. Vansant, *Chem. Commun.* **2002**, 0, 1010–1011.
- [24] a) S.D. Robertson, B.D. McNicol, J.H. De Baas, S.C. Kloet, J.W. Jenkins, *J. Catal.* **1975**, 37, 424–431; b) R. Brown, M.E. Cooper, D.A. Whan, *Appl Catal.* **1982**, 3, 177–186.
- [25] a) C. Louis, Z.X. Cheng, M. Che, *J. Phys. Chem.* **1993**, 97, 5703–5712; b) S. Sitthisa, A. Wei, D. E. Resasco, *J. Catal.* **2011**, 284, 90–101; c) P. Burattin, M. Che, C. Louis, *J. Phys. Chem. B.* **1999**, 103, 6171–6178; d) H. H. Kung, *In Studies in Surface Science and Catalysis*; Elsevier, **1989**; Vol. 45, pp 91–109.
- [26] A.A. Lemonidou, M.A. Goula, I.A. Vasalos, *Catal. Today* **1998**, 46, 175–183.
- [27] X.-P. Yu, W. Chu, N. Wang, F. Ma, *Catal Lett.* **2011**, 141, 1228–1236.
- [28] a) L. Hu, L. Lin, S. Liu, *Ind. Eng. Chem. Res.* **2014**, 53, 9969–9978; b) L. Hu, G. Zhao, W. Hao, X. Tang, Y. Sun, L. Lin, S. Liu, *RSC Adv.* **2012**, 2, 11184–11206.
- [29] A.S. Nagpure, N. Lucas, S.V. Chilukuri, *ACS Sustain. Chem. Eng.* **2015**, 3, 2909–2916.
- [30] Y. Nakagawa, M. Tamura, K. Tomishige, *ACS Catal.* **2013**, 3, 2655–2668.
- [31] A.B. Gawade, M.S. Tiwari, G.D. Yadav, *ACS Sustain. Chem. Eng.* **2016**, 4, 4113–4123.
- [32] Y. Liu, M.A. Mellmer, D.M. Alonso, J.A. Dumesic, *ChemSusChem.* **2015**, 8, 3983–3986.
- [33] J. Chen, F. Lu, J. Zhang, W. Yu, F. Wang, J. Gao, J. Xu, *ChemCatChem.* **2013**, 5, 2822–2826.
- [34] a) Y. L. Liu, C. Y. Hsieh, *J. Polym. Sci. Pol. Chem.* **2006**, 44, 905–913; b) A. Gandini, D. Coelho, M. Gomes, B. Reis, A. Silvestre, *J. Mater. Chem.* **2009**, 19, 8656–8664.
- [35] C. Moreno-castilla, F. Carrasco-marín, F.J. Maldonado-hódar, J. Rivera-utrilla, *Carbon.* **1998**, 36, 145–151.
- [36] U.J. Kim, C.A. Furtado, X. Liu, G. Chen, P.C. Eklund, *J. Am. Chem. Soc.* **2005**, 127, 15437–15445.
- [37] L. Yu, L. He, J. Chen, J. Zheng, L. Ye, H. Lin, Y. Yuan, *ChemCatChem.* **2015**, 7, 1701–1707.
- [38] D. Zhao, J. Feng, Q. Huo, N. Melosh, G.H. Fredrickson, B.F. Chmelka, G.D. Stucky, *Science.* **1998**, 279, 548–552.

**Entry for the Table of Contents** (Please choose one layout)

Layout 1:

## FULL PAPER

Non-promoted monometallic Ni/SBA-15 catalyst, prepared by Incipient Wetness Impregnation can convert HMF to 2,5-dimethylfuran (DMF) or to 2,5-dimethyltetrahydrofuran (DMTHF). Through the control over reaction time, high yields to DMF (71%, at conversion of 93%) and to DMTHF (97%, at conversion of 100%) can be achieved. The kinetic study affords the determination of a preferential reaction route from HMF to DMTHF through 5-methylfurfural (MFFR).



Shuo Chen, Carmen Ciotonea, Karine Vigier De Oliveira, François Jérôme, Robert Wojcieszak, Franck Dumeignil, Eric Marceau, \* Sebastien Royer\*

Page No. – Page No.

**Hydroconversion of 5-hydroxymethylfurfural to 2,5-dimethylfuran and 2,5-dihydroxymethyltetrahydrofuran over non-promoted Ni/SBA-15**